Journal of Photochemistry & Photobiology, B: Biology 173 (2017) 43–49

Contents lists available at ScienceDirect

Journal of Photochemistry & Photobiology, B: Biology

journal homepage: www.elsevier.com/locate/jphotobiol

Synthesis and characterization of metal oxides (CeO_2, CuO, NiO, Mn_3O_4, SnO_2 and ZnO) nanoparticles as photo catalysts for degradation of textile dyes

Lalitha Gnanasekaran[a], R. Hemamalini[a,*], R. Saravanan[b], K. Ravichandran[c], F. Gracia[b], Shilpi Agarwal[d], Vinod Kumar Gupta[d,*]

[a] Department of Physics, Queen Mary's College, Chennai 600 004, India
[b] Department of Chemical Engineering and Biotechnology, University of Chile, Beauchef, 850 Santiago, Chile.
[c] Department of Nuclear Physics, University of Madras, Guindy Campus, Chennai 600 025, India
[d] Department of Applied Chemistry, University of Johannesburg, Johannesburg, South Africa

ARTICLE INFO

Keywords:
Metal oxides
Zinc oxide
UV-light
Photocatalyst
Degradation

ABSTRACT

The progress of the enriched photocatalytic degradation predominantly depends on materials fabrication. In the recent times, the outcomes of nanomaterials show extraordinary efficiency due to its shape and size. In this connection, the present work concentrates on the fabrication of single digit metal oxides (CeO_2, CuO, NiO, Mn_3O_4, SnO_2 and ZnO) through precipitation method. The structural information of different metal oxides (MOs) and their crystallite size were estimated via XRD analysis and their consistent results revealed that the crystalline sizes of the prepared metal oxide were exhibited in nano size. The morphology and dimension of the synthesized MOs were identified through FE-SEM and TEM techniques. The FE-SEM images were apparently defined that the actual morphology of each metal oxide expresses different dimension due to nucleation and growth process. The result of UV–vis absorption spectra was helped to identify the band gap of MOs and a suitable light for photocatalytic irradiation. Additionally, the synthesized single digit MOs nanoparticles were magnificently applied for the degradation of methyl orange and methylene blue under UV light irradiation.

1. Introduction

In the past few decades, the developing countries have met the hazardous risk to the environment due to the failure of pure water supply. According to the world health organization (WHO, 2014) reports, over 10 million people were infected by various illnesses because of water contamination [1]. Recently, UN (WWAP 2016) had reported that one billion (three out of four jobs) people were mainly dependent on water related sources [2]. Therefore, pure water is a crucial factor for every creature as well as the world economy. On the other hand, the organic manufacturing industries were disposing their chemical wastes straight away into the pure water sources, which results in several environmental problems [3]. Therefore, the society must ensure proper safety measures for the essential environmental factors and sustainable development of human life.

Recently, researchers pointed toward the nanosized metal oxides based photocatalyst for its potential utility in the treatment of waste water [3–10]. While comparing both micro and bulk materials, nanosized materials show enhanced degradation efficiency since it displays excellent characteristic results via quantum confinement effect [6]. Nano metal oxides being a suitable candidate for wastewater treatment, it have been widely employed in a variety of other applications such as solar cell, fuel cell, gas sensor, hydrogen storage and generation, anti-bacterial activities and etc. [8,11–12]. Metal oxides have been showing a greater interest to synthesize with more attractive morphologies. Since the size, shape and structure of the nanosized metal oxides correlate with its properties, it has been produced with different shapes like nanospheres, nanowires, nanorods, nanocombs, nanoleaves, nanobelts etc. [13–15]. Several recent reports focused to synthesize of nanostructured metal oxides by various physical and chemical methods such as sol-gel, hydrothermal, chemical precipitation, thermal decomposition and chemical bath deposition methods [14,16]. It is of greater interest to prepare single digit metal oxide nanostructures in well-defined shapes and sizes.

The main goal of the present work is the synthesis of single digit metal oxides (MOs) nanoparticles such as zinc oxide (ZnO), copper oxide (CuO), nickel oxide (NiO), tin oxide (SnO_2), manganese oxide (Mn_3O_4) and cerium oxide (CeO_2) by the chemical precipitation

* Corresponding authors.
E-mail addresses: hemaphy.qmc@gmail.com (R. Hemamalini), vinodfcy@gmail.com, vinodg@uj.ac.za (V.K. Gupta).

http://dx.doi.org/10.1016/j.jphotobiol.2017.05.027
Received 19 April 2017; Received in revised form 18 May 2017; Accepted 19 May 2017
Available online 20 May 2017
1011-1344/

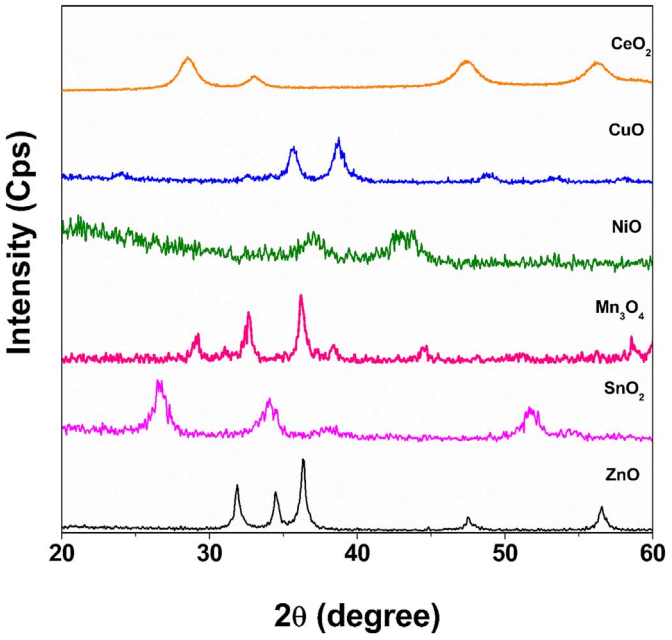

Fig. 1. The X-ray diffraction pattern of the entire synthesized MOs nanomaterials.

method. Best of the author's knowledge, this is the first report for the preparation single digit six different MOs nanomaterials. In addition, the synthesized various metal oxide properties were categorized by different techniques like X-ray diffraction (XRD), field emission scanning electron microscopy (FE-SEM), transmission electron microscopy (TEM), Energy-dispersive X-ray spectroscopy (EDS), Brunauer–Emmett–Teller (BET) and UV–vis absorption spectrophotometer (UV–vis). Likewise, the prepared metal oxides were engaged to the degradation of methyl orange and methylene blue via photocatalytic reaction under UV light irradiation.

2. Experimental Details

2.1. Materials

For the single digit MOs preparation; the following chemicals are necessary, such as Nickel (II) chloride hexahydrate ($NiCl_2{\cdot}6H_2O$), Copper (II) chloride ($CuCl_2$), Zinc chloride anhydrous ($ZnCl_2$), Cerium(III) acetate hydrate ($Ce(CH_3CO_2)_3{\cdot}H_2O$), Tin(II) chloride anhydrous ($SnCl_2$), Manganese (II) chloride tetrahydrate ($MnCl_2{\cdot}4H_2O$), sodium hydroxide (NaOH) pellets and for photocatalytic activity testing, methyl orange and methylene blue are required. Which were procured from Rankem and Sigma-Aldrich chemicals. In this procedure, the entire aqueous solution was prepared with double distilled (DD) water.

2.2. Synthesis of Single Digit MOs Nanoparticles

The existing work focuses on the synthesis of single digit MOs nanoparticles by precipitation method. While comparing with other chemical methods, chemical precipitation is a unique, cost-effective and simply available method [14,17]. In this method initially, 0.01 M of metal oxide precursors (separately) was dissolved in 400 mL of DD water in a 1000 ml beaker through persistent stirring (RPM 600) condition. After that, the alkaline solution is gradually added (in this report, we used sodium hydroxide (NaOH) is alkaline) drop wise into the above dissolved solution under constant stirring atmosphere at room temperature. Simultaneously, the pH of the above solution was monitored and sustained in-between 7 and 8. As a result, the formation of precipitates is attained. Then, the precipitation was washed numerous times with the use of DD water and allowed to dry at room temperature for a few days. Subsequently, the dried powder was calcinated at 350 °C for 30 min with a heating rate of 5 °C per minute. At the end, we have completed the successful synthesis of single digit metal oxide nanoparticles. The following chemical reaction is easily understood by the above procedure;

$$\text{MO precursor} + \text{NaOH} \rightarrow \text{MO hydroxides} + \text{NaCl} + H_2O \quad (1)$$

The precipitate powder was washed several times with the use of DD water due to removal of NaCl.

$$\text{MO hydroxides} + \text{NaCl} + H_2O \rightarrow \text{MO hydroxides} + \text{NaCl}\uparrow + H_2O \quad (2)$$

After the reaction, the above solution was filtered and dried, then the dry preserved powder was calcinated at 350 °C for 30 min.

$$\text{MO hydroxides} + H_2O \xrightarrow{\Delta} \text{single digit MO nanoparticles} + H_2O\uparrow \quad (3)$$

Finally, we obtained single digit MO nanoparticles.

2.3. Procedure for Photocatalytic Testing

The photocatalytic testing procedure was surveyed by our previous literature [18–19]. Primarily, the light (photo) stability of the degradation dyes (methyl orange and methylene blue) was tested without catalyst and their outcomes were unmistakably identified that the degradation dyes have more stable nature under UV light irradiation. Before irradiation, the photocatalytic testing solution was prepared by 100 mg of single digit MO nanocatalyst into 100 ml of dye solution (initial concentration of methyl orange and methylene blue is 5×10^{-5} mol/L) in a 1000 mL quartz container covered with a water jacket. The photocatalytic testing solution was consistently stirred with a constant RPM 600. The earliest (without light) and light exposed solutions were collected periodically (each 20 min) up to 2 h. In this process, the UV lamp (8 W, λ = 365 nm) was hold as a light source for irradiation. The initial and light exposed solutions were centrifuged, filtered for the purpose of removing the catalyst into the dye solution and then the concentration of dyes were monitored via UV–visible spectrophotometer. The effectiveness of the degradation were determined by the following formula [18–19],

$$\eta = \left[1 - \frac{C}{C_0}\right] \times 100 \quad (4)$$

where, C_0 and C are the concentrations of the initial (t = 0) and light exposed solutions for't' minutes respectively.

Table 1
Structural parameters of the entire synthesized MOs nanomaterials.

Prepared MOs	JCPDS number	Structure	Crystal system	Lattice parameters (Å)			Crystallite size (nm)
				a	b	C	
CeO_2	04-0593	Cubic	a = b = c	5.401			6.5
CuO	89-2529	Monoclinic	a ≠ b ≠ c	4.679	3.430	5.133	7.8
NiO	04-0835	Cubic	a = b = c	4.180			6.3
Mn_3O_4	89-4837	Tetragonal	a = b ≠ c	5.771		9.450	9.6
SnO_2	88-0287	Tetragonal	a = b ≠ c	4.730		3.190	6.8
ZnO	65-3411	Hexagonal	a = b ≠ c	3.240		5.210	8.1

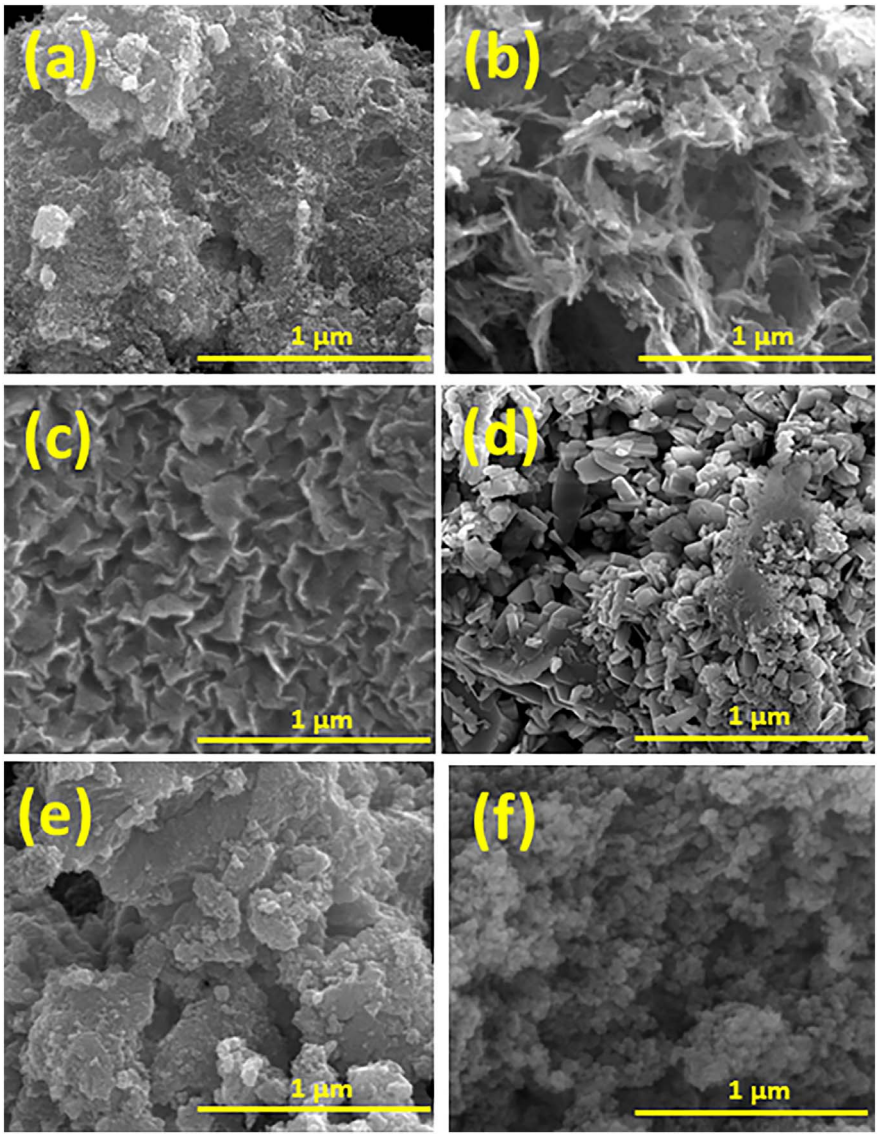

Fig. 2. FE-SEM images of (a) CeO_2, (b) CuO, (c) NiO, (d) Mn_3O_4, (e) SnO_2 and (f) ZnO nanomaterials.

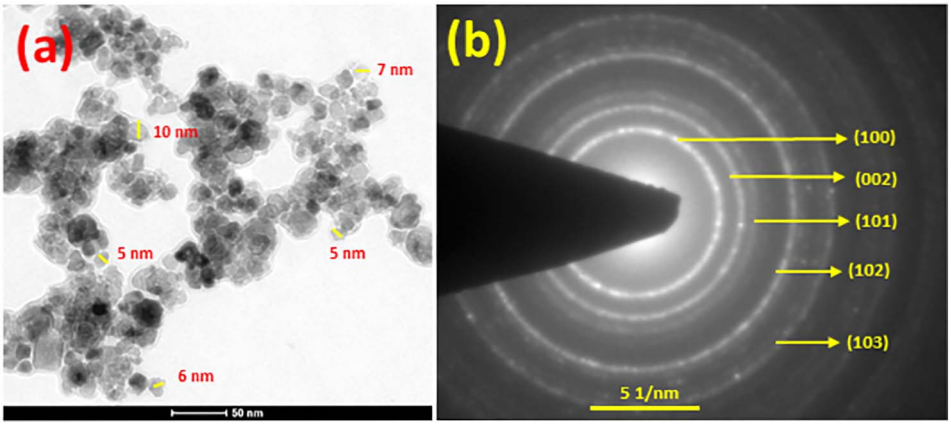

Fig. 3. (a) TEM images and (b) SAED pattern of ZnO nanomaterials.

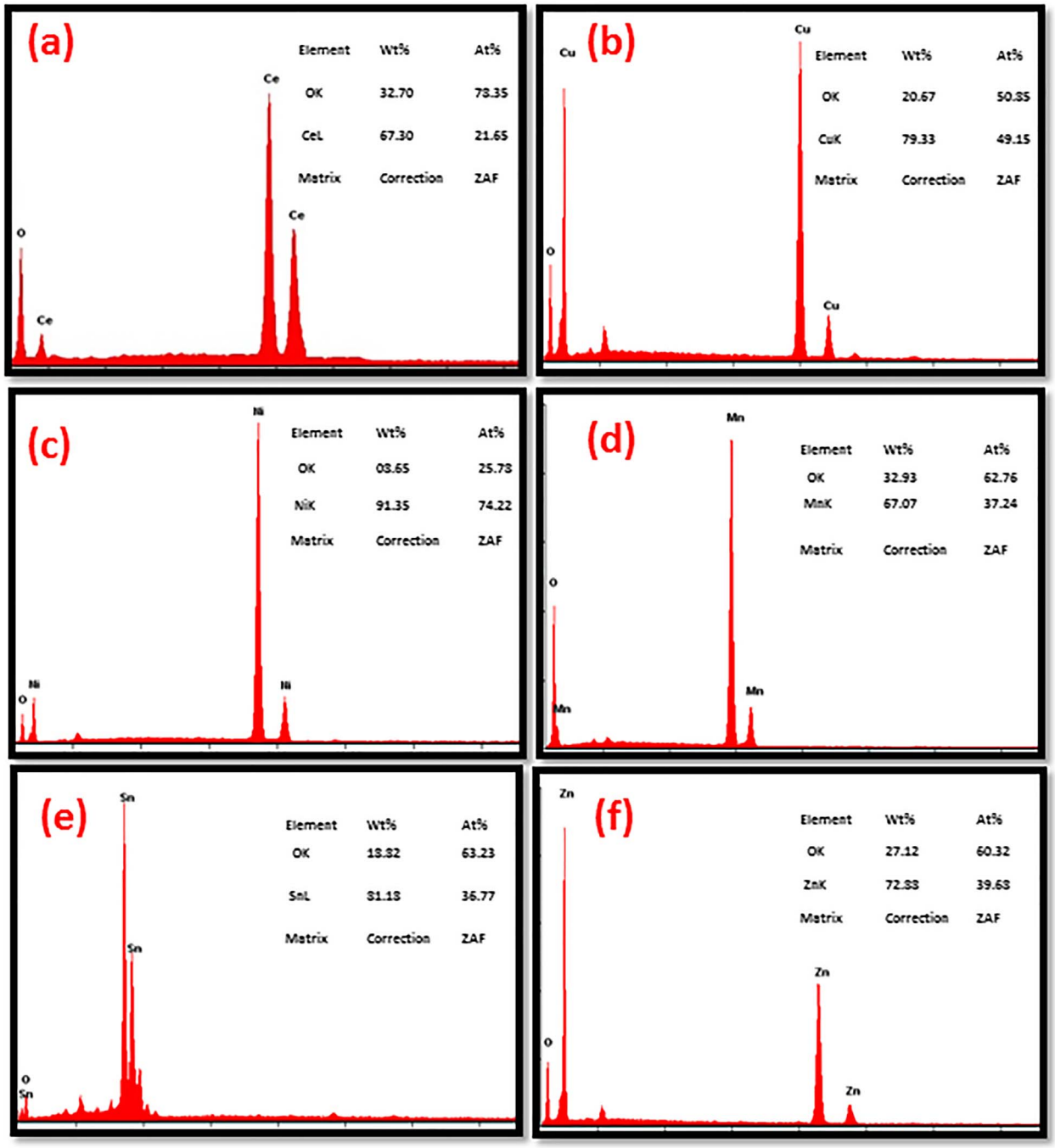

Fig. 4. EDS spectra of (a) CeO_2, (b) CuO, (c) NiO, (d) Mn_3O4, (e) SnO_2 and (f) ZnO nanomaterials.

Table 2
Surface area, absorption wavelength, band gap and degradation efficiency of the entire synthesized MOs nanomaterials.

Prepared MOs	BET surface area (m^2/g)	Absorption wavelength (λ)	Band gap (E_g)	Degradation of methyl orange (%)	Degradation of methylene blue (%)
CeO_2	76.8	371	3.34	70	77
CuO	42.5	720	1.72	12	15
NiO	40.3	327	3.83	49	55
Mn_3O_4	31.2	425	2.91	20	26
SnO_2	72.5	373	3.32	78	83
ZnO	65.8	376	3.29	93	98

2.4. Characterization Details

The lattice parameters, crystallite size and structure of the prepared single digit MOs were determined with the use of powder X-ray diffraction pattern which were carried out at room temperature ($2\theta = 20^\circ$ to 60°) by a Siemens diffractometer (D5000) with $CuK_{\alpha 1}$ radiation ($\lambda = 1.5406$ Å). The morphology and existing elements in the single digit MOs were scrutinized via field emission scanning electron microscope (FEI quanta FEG 200-FE-SEM with EDS detector) and transmission electron microscopy (TEM-Tecnai G^2 20). The value of the absorption wavelength (λ) and band gap energy (E_g) of the prepared single digit MOs were examined by UV–vis spectrophotometer (CARY 5E UV-VIS-NIR). The exact surface area of single digit MOs were

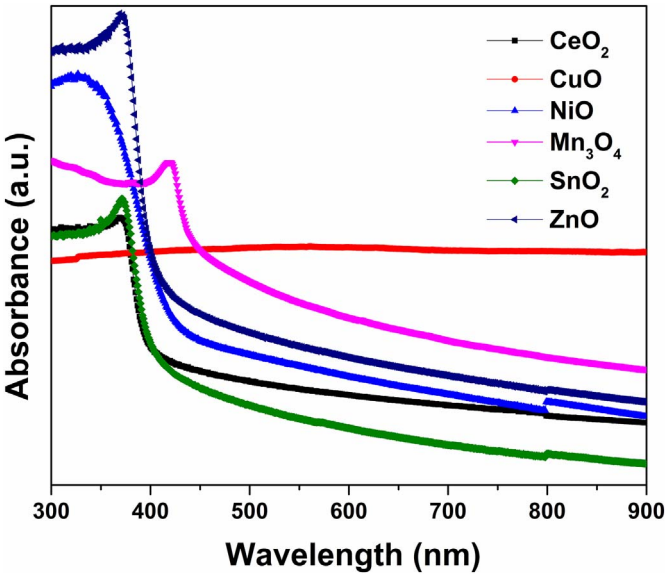

Fig. 5. UV–vis absorption spectra of all prepared MOs nanomaterials.

calculated by exhausting Brunauer–Emmett–Teller equation (BET, Micromeritics ASAP 2020, USA). The absorption value of initial and irradiated dyes such as methyl orange (464 nm) and methylene blue (664 nm) solution were monitored via Perkin – Elmer UV–visible spectrometer RX1.

3. Results and Discussions

3.1. Structural Analysis

Before the actual photocatalytic test, the invention of the properties of synthesized MOs nanomaterial was essential due to categorizing an efficient catalyst. The lattice parameter, crystallite size and structure of the synthesized MOs nanomaterials were recognized through powder X-ray diffraction pattern. The X-ray diffraction pattern of all synthesized MOs was exposed in Fig. 1. The obtained X-ray diffraction data were entirely indexed via scientific softwares like Origin 8 and XRDA 3.1. The individual indexed data of each MOs were briefly described below; the diffraction peaks of CeO_2 nanomaterial were seemed at 28.5°, 33.1°, 47.5° and 56.4° and their resultant *hkl* planes were predictable such as (111), (200), (220) and (311) respectively. The consequences plainly recognized that the CeO_2 material displays cubic structure and their dependable parameters are presented in Table 1.

The major intention of the present work is to synthesize single digit MOs which were identified through crystallite size using Scherrer formula and the values are displayed in Table 1. The CuO nanomaterial indicates monoclinic structure and their corresponding diffraction peaks were obtained at (2θ values) 35.5°, 38.6°, 48.8°, 53.3°, 58.2° parallel to ($\bar{1}11$), (111), ($\bar{2}02$), (020), (202) planes. The 2θ value of synthesized NiO nanomaterials appeared at 37.3° and 43.1° and their comparable planes are (111) and (200) which represented cubic crystal structure of NiO nanomaterials. On the other hand, the Mn_3O_4 nanomaterials reveal tetragonal structure and the scrutinized 2θ values are 28.9°, 32.3°, 36.1°, 44.4° and 59.8° that matches with (112), (103), (211), (220) and (224) planes. For SnO_2 nanomaterials, tetragonal structure is obtained and the 2θ values 26.6°, 33.9°, 37.9° and 51.8° with their equivalent planes (110), (101), (200) and (211). At the end, the diffraction pattern of ZnO parades hexagonal structure and their 2θ values 31.6°, 34.4°, 36.3°, 47.5° and 56.5° coincide with, (100), (002), (101), (102) and (110) planes. The lattice parameter and crystallite size of the entire MOs were displayed in Table 1. Hence, the X-ray diffraction results of all synthesized MOs were evidently listed pure structure without impurities and their crystallite values are seemed in single digits.

3.2. Morphological Analysis

The morphology of the prepared materials plays a dynamic part to increase the photocatalytic degradation rate. The confirmation of dimension for the prepared MOs was clarified with use of FE-SEM and TEM measurements. The FE-SEM images of the synthesized MOs were presented in Fig. 2. The outcome of MOs images apparently described that the actual morphology of each metal oxide expresses different dimension due to growth and nucleation process [20–22].

When associated with other metal oxides images, the FE-SEM image of ZnO (Fig. 2f) illustrates that the particles are identical and tiny spherical in shape. At the meantime, the FE-SEM images of CuO, NiO and Mn_3O_4 show striking morphology such as nanoleaves, nanoflowers and nanoplates which were evidently displayed in Fig. 2b, c and d respectively. On the contrary, the CeO_2 (Fig. 2a) and SnO_2 (Fig. 2e) materials exposed cluster of tiny particles due to its small size. The above statement is convenient with the XRD results. Hence, the FE-SEM results were unmistakably labelled that the synthesized MOs materials indicated dissimilar shape and dimension. Furthermore, the perfect size of the ZnO material was explored with TEM observation.

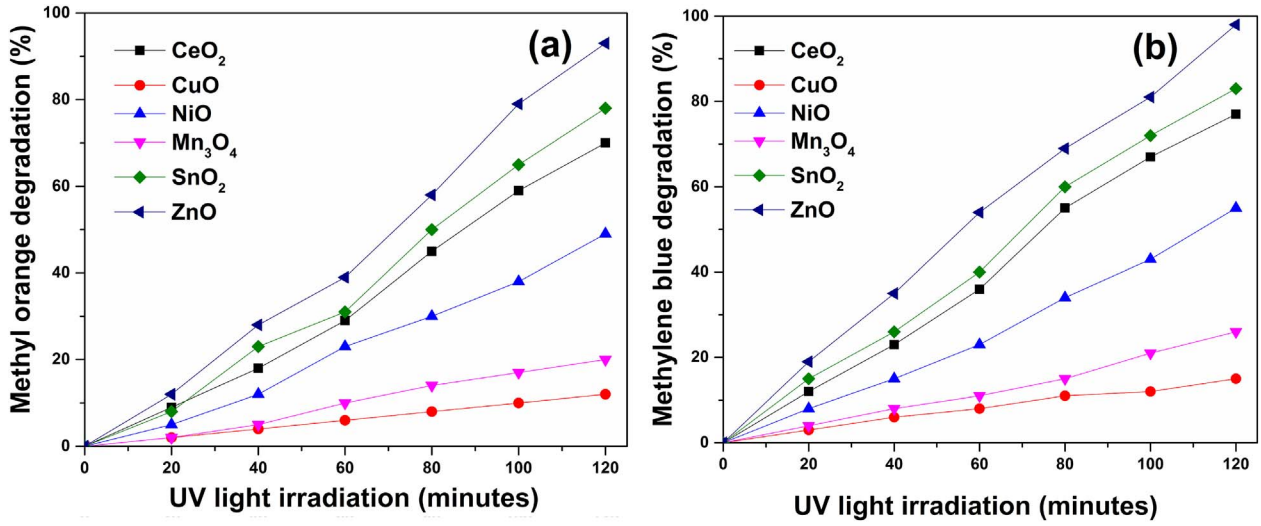

Fig. 6. Photocatalytic degradation of (a) methyl orange and (b) methylene blue under illumination of UV light using all prepared MOs nanoparticles. (For interpretation of the references to colour in this figure legend, the reader is referred to the web version of this article.)

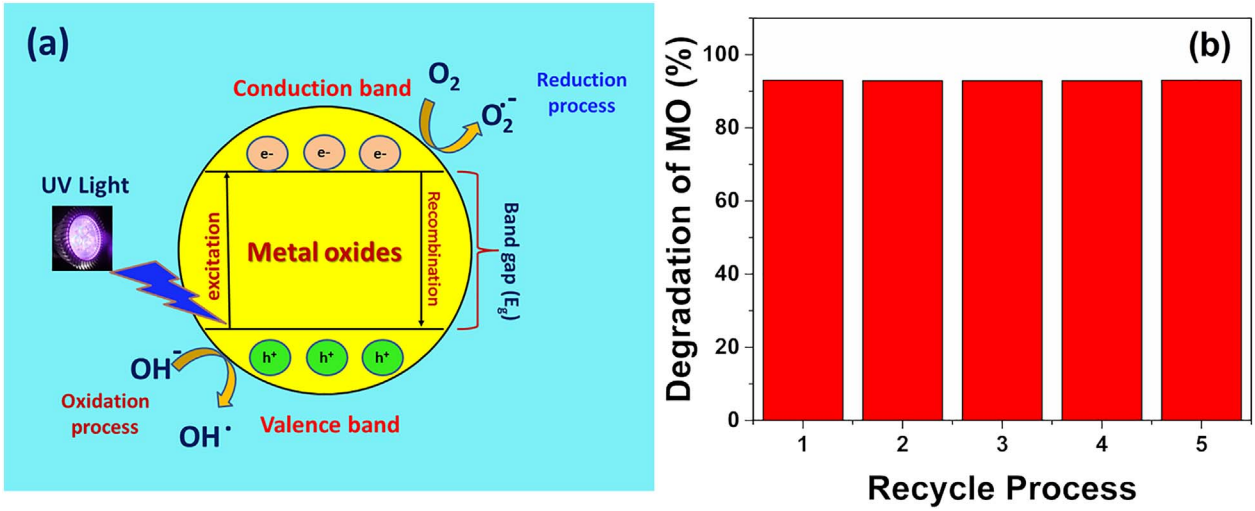

Fig. 7. (a) Schematic illustration of general photocatalytic mechanism of metal oxides materials and (b) Recycling process of MO using ZnO nanoparticles.

The TEM image of synthesized ZnO nanocatalyst was revealed in Fig. 3a. The present TEM image was undoubtedly exposed FE-SEM reflection. The prepared ZnO nanomaterials were appeared in spherical shape with an average diameter of ~8.5 nm. Based on the selected area electron diffraction rings (Fig. 3b), the d-spacing values were determined as 0.281 nm, 0.260 nm, 0.247 nm, 0.191 nm, 0.147 nm and their exactly matched *hkl* planes (100), (002), (101), (102) and (103) were recognized. The results were absolutely identified that the prepared material has exposed pure ZnO hexagonal structure. Moreover, the obtainable elements in the prepared MOs were identified with EDS spectra.

3.3. Chemical Composition and Surface Area Analysis

From Fig. 4, the EDS spectra were unmistakably showed that the prepared single digit MOs represent well purity. Furthermore, no other elements present in the spectra which indicated that the synthesized materials have their own existing elements. Finally, the chemical (weight and atomic percentage) composition of synthesized MOs was displayed on their respective EDS spectrum. The BET surface area value of each MOs was listed in Table 2. The surface area value proposed that the synthesized CeO_2 material induced superior photocatalytic degradation rate due to its large surface area while compared with other MOs. It is an already known fact that the large surface area motivates high redox reaction. This process created more electrons and holes, which energetically participate during the photocatalytic reaction and it supports to attain superior degradation rate [20,23–24].

3.4. Absorption Wavelength and Band gap Analysis

The absorption wavelength of the prepared single digit MOs were primarily influenced to isolate a suitable light for photocatalytic irradiation [25]. Therefore, the absorption wavelengths of all MOs were notorious with the help of UV–vis absorption spectra which were shown in Fig. 5. From Fig. 5, the strong absorption wavelength and band gap (Eg) values of each MOs were sharply identified and are tabulated in Table 2. The strong absorption of synthesized CeO_2, NiO, SnO_2 and ZnO nanomaterials wavelength appeared in UV region. On the other hand, the wavelength of prepared CuO and Mn_2O_3 is in visible region. Hence in the current work, maximum number of prepared materials trust on UV irradiation, so that these characteristics help to employ UV light for irradiation during degradation time.

3.5. Photocatalytic Testing

In the current work, the primarily task is to emphasis on the preparation of single digit MOs and photocatalytic degradation of methyl orange and methylene blue under illumination of UV light. Fig. 6 demonstrates the time dependent degradation attainment curve for all prepared MOs. The ultimate degradation percentages (within 2 h irradiation of UV light) of all MOs were listed in Table 2.

The result was unexpected while related with other oxides (CeO_2, CuO, NiO, Mn_3O_4 and SnO_2) result, ZnO illustrates high effective catalyst for the degradation of methyl orange and methylene blue. The outcomes visibly listed that the CuO and Mn_3O_4 materials precise slow degradation ability, due to small bandgap which is powerless to prompt more electrons and holes during the irradiation of UV light [26–28].

Fig. 7 (a) shows the graphical representation of the general photocatalytic mechanism of metal oxide materials. The photons (UV light, 365 nm) irradiate on the metal oxide surface, the valence electrons are disturbed and transfer to the conduction band of the metal oxides. On the other hand, the holes would be left in the valence band. These holes in the valence band react with water molecules to generate hydroxyl radicals [16]. Simultaneously, the conduction band electrons react with dissolved oxygen species to form superoxide ions. These holes and electrons were effectively initiated oxidation and reduction reactions to effectively produce OH radicals. The radicals play a dynamic role in decomposition of MO and MB dyes [16].

The enriched photocatalytic activity of ZnO nanomaterial depends on the following reasons: It is earlier stated that the amorphous or semi crystalline material expresses a reduced amount of degradation rate while compared with crystalline materials [29–30]. In our case, the XRD results clearly exhibited that the ZnO material has well crystalline nature. On the other hand, the shape of the prepared material performs a key role for achieving high degradation rate [16,29–32]. The morphology promotes the degradation rate, because the shape inspires on the surface property of the prepared materials [16,18–19,29–32]. The FE-SEM images endorse that the prepared CeO_2 and SnO_2 materials display aggregated bunch of particles. So, during the UV light irradiation, some of the particles were incapable to participate actively in the photocatalytic reaction that leads to reduce the activity. Meanwhile, the ZnO material was presented with spherical shape that is one of the main reasons to enrich the activity. Several literatures had described that the spherical shaped particles indicate higher degradation rate when compared to materials having other shapes [16,18–19,31,33]. So, finally we have concluded that the synthesized ZnO material have well crystalline nature with uniform spherical shape. These parameters

essentially helped to achieve a higher degradation rate. The stable and reusable properties of enhanced ZnO catalyst were clearly identified by recycling process of MO. From the Fig. 7b, the result of the 5 times recycling process of ZnO shows no significant variations in the MO degradation rate which means that the materials having good stability [34–48]. Further, the catalyst will be utilized in the industrial waste water treatments.

4. Conclusion

In this report, simple n method has facilitated the preparation of single digit metal oxides (CeO_2, CuO, NiO, Mn_3O_4, SnO_2 and ZnO) nanoparticles. The entire characterization results were assisted to identify the size, shape, chemical composition and band gap of the synthesized materials. Compared with other metal oxides (CeO_2, CuO, NiO, Mn_3O_4 and SnO_2), the photocatalytic activity of ZnO has showed superior degradation rate because of its spherical shape and crystallinity.

Acknowledgements

We acknowledge SAIF-IIT Chennai, India for characterization facilities like FE-SEM and UV–vis spectrophotometer. The authors (R.S., F.G.) acknowledge the support of CONICYT through the project CONICYT/FONDECYT/3150631 and the postdoctoral fellowship granted to R.S.

References

[1] Investing in Water and Sanitation: Increasing Access, Reducing Inequalities UN water Global Analysis and Assessment of Sanitation and Drinking-water GLASS, (2014).
[2] Water and Jobs - The UN World Water Development Report UNESCO-WWAP, (2016).
[3] J. Schneider, et al., Understanding TiO_2 photocatalysis: mechanisms and materials, Chem. Rev. 114 (19) (2014) 9919–9986.
[4] B.J. Sanghavi, et al., Ultrafast immunoassays by coupling dielectrophoretic biomarker enrichment in nanoslit channel with electrochemical detection on graphene, Lab Chip 15 (2015) 4563–4570.
[5] B.J. Sanghavi, et al., Aptamer-functionalized nanoparticles for surface immobilization-free electrochemical detection of cortisol in a microfluidic device, Biosens. Bioelectron. 78 (2016) 244–252.
[6] M.R. Hoffmann, S.T. Martin, W. Choi, D.W. Bahnemann, Environmental applications of semiconductor photocatalysis, Chem. Rev. 95 (1) (1995) 69–96.
[7] B.J. Sanghavi, et al., Electrokinetic preconcentration and detection of neuropeptides at patterned graphene-modified electrodes in a nanochannel, Anal. Chem. 86 (2014) 4120–4125.
[8] J. Liqiang, et al., Review of surface photovoltage spectra of nano-sized semiconductor and its applications in heterogeneous photocatalysis, Sol. Energy Mater. Sol. Cells 79 (2) (2003) 133–151.
[9] B.J. Sanghavi, et al., Real-time electrochemical monitoring of adenosine triphosphate in the picomolar to micromolar range using graphene-modified electrodes, Anal. Chem. 85 (2013) 8158–8165.
[10] B.J. Sanghavi, et al., Potentiometric stripping analysis of methyl and ethyl parathion employing carbon nanoparticles and halloysite nanoclay modified carbon paste electrode, Anal. Chim. Acta 735 (2012) 37–45.
[11] X. Yu, T.J. Marks, A. Facchetti, Metal oxides for optoelectronic applications, Nat. Mater. 15 (2016) 383–396.
[12] Y. Ren, Z. Ma, P.G. Bruce, Ordered mesoporous metal oxides: synthesis and applications, Chem. Soc. Rev. 41 (2012) 4909–4927.
[13] P.R. Solanki, A. Kaushik, V.V. Agrawal, B.D. Malhotra, Nanostructured metal oxide-based biosensors, NPG Asia Mater. 3 (2011) 17–24.
[14] T. Guo, M.S. Yao, Y.H. Lin, C.W. Nan, A comprehensive review on synthesis methods for transition-metal oxide nanostructures, CrystEngComm 17 (2015) 3551–3585.
[15] R.S. Devan, R.A. Patil, J.H. Lin, Y.R. Ma, One-dimensional metal-oxide nanostructures: recent developments in synthesis, characterization, and applications, Adv. Funct. Mater. 22 (16) (2012) 3326–3370.
[16] R. Saravanan, V.K. Gupta, V. Narayanan, A. Stephen, Comparative study on photocatalytic activity of ZnO prepared by different methods, J. Mol. Liq. 181 (2013) 133–141.
[17] R. Salomão, L.M. Milena, M.H. Wakamatsu, V.C. Pandolfelli, Hydrotalcite synthesis via co-precipitation reactions using MgO and $Al(OH)_3$ precursors, Ceram. Int. 37 (8) (2011) 3063–3070.
[18] L. Gnanasekaran, R. Hemamalini, K. Ravichandran, Synthesis and characterization of TiO_2 quantum dots for photocatalytic application, J. Saudi Chem. Soc. 19 (5) (2015) 589–594.
[19] L. Gnanasekaran, et al., Intermediate state created by dopant ions (Mn, Co and Zr) into TiO_2 nanoparticles for degradation of dyes under visible light, J. Mol. Liq. 223 (2016) 652–659.
[20] G.H. Han, et al., Influence of copper morphology in forming nucleation seeds for graphene growth, Nano Lett. 11 (10) (2011) 4144–4148.
[21] K. Jayanthi, S. Chawla, K.N. Sood, M. Chhibara, S. Singh, Dopant induced morphology changes in ZnO nanocrystals, Appl. Surf. Sci. 255 (2009) 5869–5875.
[22] S.J. Cox, Z. Raza, S.M. Kathmann, B. Slater, A. Michaelides, The microscopic features of heterogeneous ice nucleation may affect the macroscopic morphology of atmospheric ice crystals, Faraday Discuss. 167 (2013) 389–403.
[23] X. Yang, Y. Wang, L. Xu, X. Yu, Y. Guo, Silver and indium oxide codoped TiO_2 nanocomposites with enhanced photocatalytic activity, J. Phys. Chem. C 112 (2008) 11481–11489.
[24] V. Ramaswamy, N.B. Jagtap, S. Vijayanand, D.S. Bhange, P.S. Awati, Photocatalytic decomposition of methylene blue on nanocrystalline titania prepared by different methods, Mater. Res. Bull. 43 (2008) 1145–1152.
[25] R. Saravanan, et al., ZnO/Ag/CdO nanocomposite for visible light-induced photocatalytic degradation of industrial textile effluents, J. Colloid Interface Sci. 452 (2015) 126–133.
[26] Z. Luo, et al., Improved photocatalytic activity and mechanism of Cu_2O/N–TiO_2 prepared by a two-step method, RSC Adv. 4 (2014) 17797–17804.
[27] A.A. Amer, S.M. Reda, M.A. Mousa, M.M. Mohamed, Mn_3O_4/graphene nanocomposites: outstanding performances as highly efficient photocatalysts and microwave absorbers, RSC Adv. 7 (2017) 826–839.
[28] V.K. Gupta, A.K. Singh, L.K. Kumawat, Thiazole Schiff base Turn-On Fluorescent Chemosensor for Al_{3+} Ion, Sensors & Actuators: B. Chemical 195 (2014) 98–108.
[29] V.K. Gupta, et al., Degradation of azo dyes under different wavelengths of UV light with chitosan-SnO2 nanocomposites, J. Mol. Liq. 232 (2017) 423–430.
[30] R. Saravanan, et al., Conducting PANI stimulated ZnO system for visible light photocatalytic degradation of coloured dyes, J. Mol. Liq. 221 (2016) 1029–1033.
[31] Y. Wang, X. Li, G. Lu, G. Chen, Y. Chen, Synthesis and photo-catalytic degradation property of nanostructured-ZnO with different morphology, Mater. Lett. 62 (2008) 2359–2362.
[32] H. Wang, C. Xie, W. Zhang, S. Cai, Z. Yang, Y. Gui, Comparison of dye degradation efficiency using ZnO powders with various size scales, J. Hazard. Mater. 141 (2007) 645–652.
[33] R. Saravanan, H. Shankar, G. Rajasudha, A. Stephen, Photocatalytic degradation of organic dye using nano ZnO, Int. J. Nanosci. 10 (1–2) (2011) 253–257.
[34] R. Saravanan, et al., Ce^{3+}-ion-induced visible-light photocatalytic degradation and electrochemical activity of ZnO/CeO2 nanocomposite, Nat. Sci. Rep. 6 (2016) 31641.
[35] T.A. Saleh, V.K. Gupta, Processing Methods and Characteristics of Porous Carbons Derived from Waste Rubber Tires: A Review, Adv. Colloid Interf. Sci. 211 (2014) 93–101.
[36] V.K. Gupta, R. Kumar, A. Nayak, T.A. Saleh, M.A. Barakat, Adsorptive removal of dyes from aqueous solutions onto carbon nanotubes: A review, Adv. Colloid Interf. Sci. (2013) 24–34.
[37] V.K. Gupta, T.A. Saleh, Sorption of Pollutants by Porous Carbon, Carbon Nanotubes and fullerene: an overview, Environ. Sci. Pollut. Res. 20 (2013) 2828–2843.
[38] V.K. Gupta, I. Ali, T.A. Saleh, A. Nayak, S. Agarwal, Chemical Treatment Technologies for Wastewater Recycling –a Review, RSC Adv. 2 (2012) 6380–6388.
[39] V.K. Gupta, M.R. Ganjali, P. Norouzi, H. Khani, A. Nayak, Shilpi Agarwal, Electrochemical Analysis of some Toxic Metals and Drugs by Ion Selective Electrodes, Crit. Rev. Anal. Chem. 41 (2011) 282–313.
[40] M. Ahmaruzzaman, V.K. Gupta, Rice husk and its ash as low-cost adsorbents in water and wastewater treatment, Ind. Eng. Chem. Res. 50 (2011) 13589–13613.
[41] V.K. Gupta, A. Nayak, S. Agarwal, Bioadsorbents for remediation of heavy metals: Current status and their future prospects, Environ. Eng. Res. 20 (1) (2015) 001–018.
[42] Tawfik A. Saleh, Shilpi Agarwal, V.K. Gupta, Synthesis of MWCNT/MnO2 Composites and their application for simultaneous oxidation of arsenite and sorption of arsenate, Appl. Catal. B Environ. 106 (2011) 46–53.
[43] V.K. Gupta, Tawfik A. Saleh, Functionalization of Tungsten Oxide into MWCNT and its Application as a novel Catalyst for Sun-Light-Induced Degradation of Rhodamine B, J. Colloids Interface Sci. 362 (2011) 337–344.
[44] R. Saravanan, S. Karthikeyan, V.K. Gupta, G. Sekaran, V. Narayanan, A. Stephen, Enhanced photocatalytic activity of ZnO/CuO nanocomposites for the degradation of textile dye on visible light illumination, Mater. Sci. Eng. C 33 (2013) 91–98.
[45] V.K. Gupta, A. Mittal, D. Jhare, J. Mittal, Batch and Bulk Removal of Hazardous Colouring Agent Rose Bengal by Bottom Ash, RSC Adv 2 (2012) 8381–8389.
[46] V.K. Gupta, B. Sethi, R.A. Sharma, Shilpi Agarwal, Arvind Bharti, Mercury Selective Potentiometric Sensor based on Low Rim Functionalized thiacalix [4] arene as a Cationic Receptor, J. Mol. Liq. 177 (2013) 114–118.
[47] V.K. Gupta, S. Kumar, R. Singh, L.P. Singh, S.K. Shoora, B. Sethi, Cadmium (II) ion Sensing through p-tert-butyl calix[6]arene Based Potentiometric Sensor, J. Mol. Liq. 195 (2014) 65–68.
[48] S. Karthikeyan, V.K. Gupta, R. Boopathy, A. Titus, G. Sekaran, A new approach for the degradation of aniline by mesoporous activated carbon as a heterogeneous catalyst: Kinetic and spectroscopic studies, J. Mol. Liq. 173 (2012) 153–163.